

# Effects of pore-channel ordering on the mechanical properties of anodic aluminum oxide nano-honeycombs

K.Y. Ng\* and A.H.W. Ngan

*Department of Mechanical Engineering, The University of Hong Kong, Pokfulam Road, Hong Kong, People's Republic of China*

Received 1 November 2011; revised 6 December 2011; accepted 6 December 2011

Available online 15 December 2011

The mechanical properties of anodic aluminum oxide (AAO) nano-honeycombs with different spatial ordering of pore-channels are investigated by nanoindentation. The pore-channel ordering is systematically varied by carefully adjusting the orientation of the aluminum used for anodization. The results indicate that the strength of AAO structures increases significantly with the regularity of their pore-channel arrangement, whereas the elastic modulus is less sensitive to pore-channel regularity.  
© 2011 Acta Materialia Inc. Published by Elsevier Ltd. All rights reserved.

**Keywords:** Anodic aluminum oxide; Grain orientation; Plastic deformation; Nanoindentation

Anodic aluminum oxide (AAO) produced using electrochemical oxidation of aluminum exhibits a unique nano-honeycomb structure in which straight pore-channels of diameters often less than 100 nm may extend over lengths exceeding 100  $\mu\text{m}$  [1–3]. AAO is considered to be an important material in nanotechnology fabrication, and is used as a template for the fabrication of other nanostructures such as nanotube and nanowire arrays [4–9], as well as in making functional devices such as electro-osmotic pumps [10] and gas sensors [11]. Two recent developments should help accelerate the industrial exploitation of this material: firstly, Lee et al. [12] developed a “hard anodization” approach to fabricate AAO many times faster conventional methods; and secondly, we [13] developed a method of obtaining AAO structures with selective ordering of the pore-channels homogeneously over  $\text{mm}^2$ -to- $\text{cm}^2$  areas. We discovered that, in the two-step anodization method [1] in oxalic acid, AAO films grown on top of large [001]-oriented recrystallized aluminum grains exhibited an arrangement of the pore-channels close to ideal close-packing in a domain structure, whereas that in films grown on [101] grains did not show any resemblance to close packing at all, and other orientations of the substrate aluminum yielded intermediate pore ordering [13]. This method of carefully adjusting the orientation of the aluminum substrate enables the ordering of the pore-channels in the AAO nano-honeycomb structure to be actively con-

trolled over unprecedented large areas. This is important for the fabrication of structures and devices with consistent performance, and also allows systematic investigation of the properties of AAO vs. the spatial ordering of the pore-channels.

In this paper, we report an investigation on the mechanical properties of AAO with varying pore-channel ordering. Although the mechanical behavior of macroscopic honeycomb structures has received a lot of interest in the mechanics community [14–19], the mechanical properties of AAO nanohoneycombs have been much less studied. We recently investigated the nanoindentation [20] as well as uniaxial compressive [21] behavior of AAO with non-specific pore-channel ordering. In this paper, we focus on elucidating the effects of pore-channel ordering on the nanoindentation behavior of AAO.

To establish the conditions for producing AAO structures with homogeneous pore-channel ordering over large areas, a 3 mm thick aluminum slab with purity >99.9999% [13] was chosen as the starting material. This slab was subjected to a series of thermomechanical treatments with the purpose of achieving large recrystallized grains in the mm-to-cm size range. The procedure included first cold rolling the aluminum slab to give a 10% thickness reduction, followed by an initial annealing step at 450 °C for 2 h, and then a second annealing step at 550 °C for 2 days, in a vacuum better than  $10^{-7}$  torr. The heat-treated slab was then cut into discs 1 inch in diameter by electric discharge machining, and these discs were then annealed again to remove any residual stresses.

\* Corresponding author. E-mail: [kycng@hku.hk](mailto:kycng@hku.hk)

To produce the necessary smooth surface for the later electro-anodization process, the discs were first mechanically polished with 240, 600, 1200, 2400 and 4000 grit SiC sandpapers in succession, and then electropolished in an electrolyte of 20% perchloric acid in ethanol at 20 V DC and  $-10^{\circ}\text{C}$ . The pretreated aluminum discs were then subjected to anodization in a 0.3 M oxalic acid solution at 40 V DC in a constant temperature environment of  $17 \pm 0.1^{\circ}\text{C}$  provided by an electronic feedback waterbath. A two-step anodization method [1] was employed to further improve the quality of the AAO films [13]. Here, an initial layer of AAO was formed in a first anodization step which lasted typically for about 15 h. This layer was then dissolved away by a phosphochromic acid solution (1.5 wt.%  $\text{H}_2\text{CrO}_4$  in 6 wt.%  $\text{H}_3\text{PO}_4$ ), leaving behind more regular dimpled pits on the metal substrate which acted as seeds for the growth of more regular pore channels in a second anodization step, which typically lasted for 10 h. As in our previous work [13], the as-prepared AAO structures were found to develop pore-channel ordering highly specific to the orientation of the underlying Al grain. Scanning electron microscopy (SEM) examination showed that the pore-channel ordering was uniform over the entire area of each underlying Al grain, which was from a few  $\text{mm}^2$  to a few  $\text{cm}^2$  in size, and the pore-channel ordering was different over differently orientated Al grains [13].

Nanoindentation was carried out on the AAO structures supported by their aluminum substrates in a Nanohardness Tester (CSEM, Switzerland) with a Berkovich diamond tip. An exponential loading profile was used in which the load  $P$  varied with time  $t$  according to  $P = P_0 \exp(\kappa t)$ , and this should correspond to a constant-strain-rate condition [22] with the indentation strain rate equal to  $\kappa/2$ . The constant  $\kappa$  was set to be  $0.007675 \text{ s}^{-1}$  for the load ramp, and at the maximum load, which was 50 mN, the load was held for 1 min, followed by unloading to 10% of the maximum load at a rate of  $50 \text{ mN min}^{-1}$ . The load was held at the 10% value for another 1 min in order to estimate the thermal drift rate during the testing period, followed by complete unload. At least 15 indentation tests were performed on a single grain, and altogether more than 30 grains were studied.

The AAO structures before and after nanoindentation were examined by SEM in a LEO 1530 FEG-SEM, as well as by transmission electron microscopy (TEM) in a Tecnai 20. Longitudinal sections of the AAO structures parallel to the pore-channels for both SEM and TEM were made by focused-ion-beam (FIB) milling in an FEI Quanta 3D FIB system.

Figure 1a–c shows plan-view SEM micrographs of three AAO structures with decreasing degrees of spatial ordering of the pore-channels from (a) to (c). By dissolving away the AAO film with a phosphochromic acid solution in order to expose the underlying aluminum for orientation measurement by electron backscattered diffraction, the orientations of the substrate Al grains in these three situations were determined to be [106], [125] and [011], respectively. In a recent report [13], over 100 grains were analyzed this way, and a similar relation was consistently observed: high ordering of AAO pore-channels, similar to that in Figure 1a, was observed on [001]-oriented grains, and poor ordering

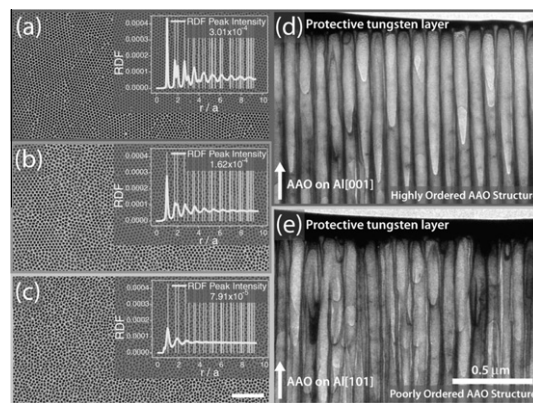


**Figure 1.** (a–c) Plan-view SEM morphology of (a) highly ordered AAO on [106] Al substrate (RDF index:  $3.013 \times 10^{-4}$  (95%)); (b) intermediate ordered AAO on [125] Al substrate (RDF index:  $1.623 \times 10^{-4}$  (54%)); and (c) poorly ordered AAO on [011] Al substrate (RDF index:  $7.913 \times 10^{-5}$  (26%)). (d and e) TEM micrographs showing the longitudinal sectional pore-channel morphology of (d) a highly ordered and (e) a poorly ordered AAO structures.

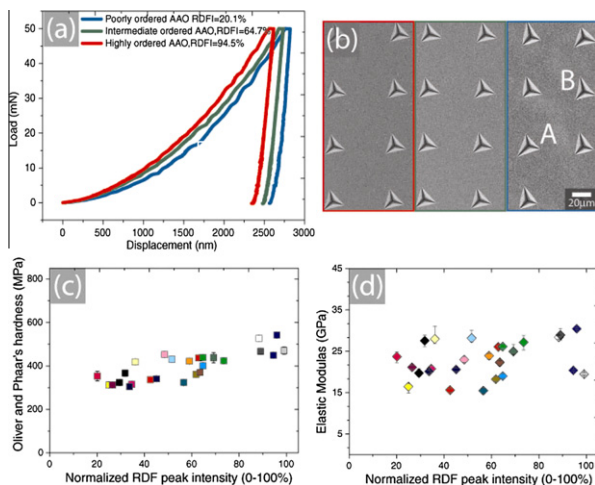
of pore-channels, similar to Figure 1c, was observed on [011]-oriented grains. The highly ordered case in Figure 1a exhibits close packing of the pore-channels in domains of a few microns wide. However, the poorly ordered case in Figure 1c does not show any resemblance to a close-packed arrangement. To quantify the pore-channel ordering, the relative positions of the pores as seen in plan-view SEM images were identified by the image-processing software ImageJ v. 1.42. This software was used to search the pixel coordinates of the centroids of the individual pores, which were then used to calculate the 2-D radial distribution function (RDF) of the pore pattern. The RDF is defined as  $[dF(r)/dr]/(2\pi r)$ , where  $F(r)$  is the fraction of pore pairs  $i$ - $j$  with center-to-center inter-pore distances  $r_{ij}$  smaller than or equal to  $r$ . The corresponding RDFs of the three structures are shown as insets in Figure 1a–c. The peaks in such an RDF correspond to the regularity of the pore positions, whereas the background joining the troughs of the peaks is due to the irregularity of the pores. Thus, a measure of the pore ordering is the area sandwiched between the RDF and the smooth background, and is termed the “RDF peak intensity” [13]. In the following, the RDF peak intensity is also expressed as a percentage normalized by the maximum value encountered in our study. The RDF peak intensity and the normalized value (blanketed) was determined to be  $3.013 \times 10^{-4}$  (95%),  $1.623 \times 10^{-4}$  (54%) and  $7.913 \times 10^{-5}$  (26%) for the three cases in Figure 1a–c, respectively; these indicators are consistent with the ordering seen in the SEM images. Figure 1d and e shows longitudinal-section TEM images of the highly ordered AAO structure grown on top of the [106]-oriented Al grain, and the poorly ordered structure on top of the [011]-oriented grain, respectively. The contrast in these two images is due to absorption by the amorphous alumina channel walls. It can be seen that the pore-channels in Figure 1d are straight and parallel, while those in Figure 1e have a strong tendency to tilt and merge.

Figure 2a shows the representative nanoindentation load–displacement curves of AAO structures with three

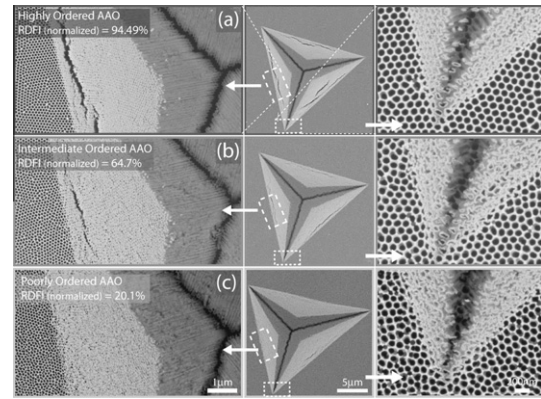
different orderings. Serrations are observed, but in terms of these, there is no significant difference between the different pore orderings. The most obvious effect is that the highly ordered structure (with RDF peak intensity = 94.5%) is significantly harder than the poorly ordered structure. Figure 2c and d summarizes the hardness and elastic modulus measured using the Oliver–Pharr method [23] from all the AAO structures investigated, versus their RDF peak intensity values. The hardness of the AAO in Figure 2c clearly increases with the pore-channel ordering. However, the measured elastic moduli of the AAO structures in Figure 2d do not show a clear trend with the pore-channel ordering.

Figure 2b shows plan-view SEM images of the nanoindentation arrays made on the AAO structures with different pore ordering. It is interesting to see that while the indents in the highly ordered case on the left are equilateral triangular in shape, those in the poorly ordered case on the right have triangular shapes which are not equilateral but elongated in different directions. For example, indent A in the poorly ordered case elongates along the 7:30 o'clock direction, while indent B elongates along the 11:00 o'clock direction. The inconsistency in the indent shape in the poorly ordered case is unlikely to be due to undulation of the AAO surface, which is estimated to be 1–2  $\mu\text{m}$  at most. It is more likely a manifestation of the random arrangement of the pore-channels in this case.

The high-magnification plan-view SEM images in Figure 3 show the details of the deformation in single indents. The tri-star shape of the plan-view structure is consistent with our earlier observation [20] that two different deformation modes, one for a region closer to the indent center and the other for a region further away from it, occurred. The deformation closer to the indent center corresponds to severe compaction of the porous AAO structure, whereas that further away from the indent center is milder and corresponds to tilting of the pore-channel walls instead of full collapse of the struc-



**Figure 2.** (a) Nanoindentation load–displacement curves of AAO structures with three different orderings. (b) SEM images of the nanoindentation arrays made on the AAO structures with different pore orderings. (c and d) Oliver–Pharr hardness (c) and elastic modulus (d) versus the RDF peak intensity values of the AAO structures studied.



**Figure 3.** The high-magnification plan-view SEM images of three AAO structures of different pore-channel ordering.

ture. The cross-sectional SEM images in Figure 4 confirm these two deformation modes of full compaction near the indent center and channel-wall tilting near the indent rim region. Again, as was observed previously [20], a sharp elastoplastic boundary exists in all the indents shown.

In a series of papers [24–27], Chung et al. studied the strength of 3-D networks and found that the correlation length is the predominant parameter that determines the failure stress under uniaxial stress. In the present work, the total area of the pores in the AAO structures was found to decrease as the pore ordering decreased. As an indication, the three AAO structures in Figure 1a–c had average pore sizes of  $75 \pm 5$ ,  $69 \pm 10$  and  $59 \pm 20$  nm, respectively, and average wall thicknesses of  $15 \pm 5$ ,  $18 \pm 10$  and  $25 \pm 15$  nm, respectively. In other words, more disordered AAO structures possess higher solid volume compared to ordered ones, and they might be expected to be stronger under load. However, the measured hardness was found to exhibit the opposite trend: for the three structures in Figure 1a–c, the hardness was  $470 \pm 20$ ,  $422 \pm 15$  and  $353 \pm 30$  MPa, respectively, i.e. more disordered structures were weaker. The results here suggest that pore-channel ordering has a significant influence on the strength of the AAO structures, and this influence cannot be described as an effect of a mean correlation length alone. Instead, the results show that the spread (i.e. variance) of the correlation length is a significant factor, i.e. a more regular arrangement of the pore-channels results in a stronger structure, and vice versa. This is not surprising, as in a more disordered

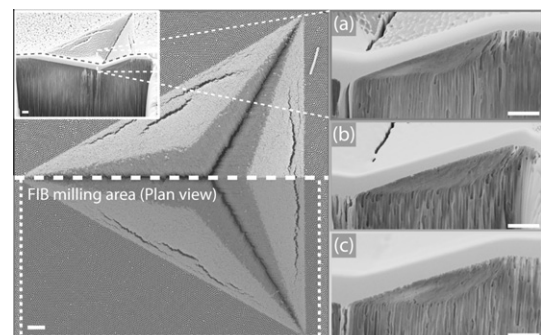


**Figure 4.** The cross-sectional SEM images of the three AAO structures in Figure 3.



structure, the stress distribution due to a given external load situation will be more non-uniform, with greater chance of occurrence of extreme stress values at locations of stress raisers. Since failure should start at locations with extreme stress values, a disordered structure should be weaker than an ordered structure. One of us performed finite-element simulations on elastic networks with varying ordering [18], and found that the statistical distribution of the internal forces indeed is a strong signature of the structure's regularity. Yield locus analysis also shows that, when subjected to the same overall load, irregular structures are weaker than regular structures [19]. The present hardness results in Figure 2c illustrate this phenomenon very well. As discussed before, the inconsistency of the indent shape in the irregular AAO structure in Figure 3 is also a likely consequence of the structural irregularity. The more pronounced tilting, branching and merging of the pore-channels in a more poorly ordered structure (see Figures 1e and 4) are likely to result in large local stress concentrators, and when one of these is interacted upon by an indentation field, more severe deformation will occur there, leading to more anisotropic deformation and elongation of the indent shape along one direction. On the other hand, the elastic modulus (Figure 2d) is less affected by such stress concentration effects. The present results illustrate that the spatial ordering of the pore-channels is an important factor governing the mechanical strength of AAO. With the present technique to control the pore-channel ordering by substrate conditioning during anodization, other properties of AAO structures can be investigated systematically as a function of their pore-channel ordering.

In summary, this work illustrates a novel method that involves carefully adjusting the orientation of the aluminum substrate used for anodization, to produce AAO structures with tunable and homogeneous pore-channel ordering over mm<sup>2</sup>-to-cm<sup>2</sup> areas. Nanoindentation tests on these AAO structures with controlled pore-channel ordering indicate that their strength increases significantly with the regularity of their pore-channel arrangement.

The authors thank Prof. B.J. Duggan for kindly providing the aluminum slabs used in this study. The work described in this paper was supported by grants from the Research Grants Council (Project No. HKU7159/10E), as well as from the University Grants Committee (Project No. SEG-HKU06) of the Hong Kong Special Administration Region, PR China.

- [1] H. Masuda, K. Fukuda, *Science* 268 (1995) (1466).
- [2] H. Masuda, F. Hasegawa, S. Ono, *J. Electrochem. Soc.* 144 (1997) L127.

- [3] H. Masuda, H. Yamada, M. Satoh, H. Asoh, M. Naka, T. Tamamura, *Appl. Phys. Lett.* 71 (1997) 2770.
- [4] W.C. Hu, D.W. Gong, Z. Chen, L.M. Yuan, K. Saito, C.A. Grimes, P. Kichambare, *Appl. Phys. Lett.* 79 (2001) 3083.
- [5] Y. Zhang, G.H. Li, Y.C. Wu, B. Zhang, W.H. Song, L. Zhang, *Adv. Mater.* 14 (2002) 1227.
- [6] M.J. Zheng, L.D. Zhang, X.Y. Zhang, J. Zhang, G.H. Li, *Chem. Phys. Lett.* 334 (2001) 298.
- [7] M.S. Sander, A.L. Prieto, R. Gronsky, T. Sands, A.M. Stacy, *Adv. Mater.* 14 (2002) 665.
- [8] M.S. Sander, R. Gronsky, T. Sands, A.M. Stacy, *Chem. Mater.* 15 (2003) 335.
- [9] Y. Li, G.S. Cheng, L.D. Zhang, *J. Mater. Res.* 15 (2000) 2305.
- [10] S.K. Vajandar et al., *Nanotechnology* 18 (2007).
- [11] O.K. Varghese, D.W. Gong, W.R. Dreschel, K.G. Ong, C.A. Grimes, *Sens. Actuators, B* 94 (2003) 27.
- [12] W. Lee, R. Ji, U. Gosele, K. Nielsch, *Nat. Mater.* 5 (2006) 741.
- [13] K.Y. Ng, A.H.W. Ngan, *Chem. Mater.* 23 (2011) 5264.
- [14] T.C. Triantafillou, J. Zhang, T.L. Shercliff, L.J. Gibson, M.F. Ashby, *Int. J. Mech. Sci.* 31 (1989) 665.
- [15] I.G. Masters, K.E. Evans, *Compos. Struct.* 35 (1996) 403.
- [16] L.J. Gibson, M.F. Ashby, J. Zhang, T.C. Triantafillou, *Int. J. Mech. Sci.* 31 (1989) 635.
- [17] C. Chen, T.J. Lu, N.A. Fleck, *J. Mech. Phys. Solid* 47 (1999) 2235.
- [18] A.H.W. Ngan, *Proc. Roy. Soc. Lond. A* 461 (2005) 433.
- [19] A.H.W. Ngan, *Proc. Roy. Soc. Lond. A* 461 (2005) 1423.
- [20] K.Y. Ng, Y. Lin, A.H.W. Ngan, *Acta Mater.* 57 (2009) 2710.
- [21] K.Y. Ng, Y. Lin, A.H.W. Ngan, *J. Mech. Phys. Solids* 59 (2011) 251.
- [22] B.N. Lucas, W.C. Oliver, *Metal. Mater. Trans.* 30A (1999) 601.
- [23] W.C. Oliver, G.M. Pharr, *J. Mater. Res.* 7 (1992) 1564.
- [24] J.W. Chung, A. Roos, J.Th.M. De Hosson, *Phys. Rev. B* 54 (1996) 15094.
- [25] J.W. Chung, J.Th.M. De Hosson, E. Van der Giessen, *Phys. Rev. B* 64 (2001) 064202.
- [26] J.W. Chung, J.Th.M. De Hosson, E. van der Giessen, *Phys. Rev. B* 65 (2002) 094104.
- [27] J.W. Chung, J.Th.M. De Hosson, *Phys. Rev. B* 66 (2002) 064206.